

# Zero-Temperature Coarsening in the 2D Long-Range Ising Model

Henrik Christiansen,<sup>\*</sup> Suman Majumder,<sup>†</sup> and Wolfhard Janke<sup>‡</sup>

*Institut für Theoretische Physik, Universität Leipzig, IPF 231101, 04081 Leipzig, Germany*

(Dated: November 13, 2020)

We investigate the nonequilibrium dynamics following a quench to zero temperature of the Ising model with power-law decaying long-range interactions  $\propto 1/r^{d+\sigma}$  in  $d = 2$  spatial dimensions. The zero-temperature coarsening is always of special interest among nonequilibrium processes, because often peculiar behavior is observed. We provide estimates of the nonequilibrium exponents, viz., the growth exponent  $\alpha$ , the persistence exponent  $\theta$ , and the fractal dimension  $d_f$ . It is found that the growth exponent  $\alpha \approx 3/4$  is independent of  $\sigma$  and different from  $\alpha = 1/2$  as expected for truly short-range systems. In the short-range regime of the tunable interactions only the fractal dimension  $d_f$  of the nearest-neighbor Ising model is recovered, while the other exponents differ significantly. For the system to achieve this, the persistence exponent  $\theta$  is observed altered accordingly to  $d - d_f = \theta/\alpha$ . This relation has been proposed for annihilation processes and later numerically tested for the  $d = 2$  nearest-neighbor Ising model. We confirm this relation for all  $\sigma$  studied, reinforcing its general validity.

## I. INTRODUCTION

The nonequilibrium dynamics of systems quenched from a random start configuration to an ordered state is of fundamental interest and has been studied in numerous systems, ranging, e.g., from spin systems [1–3] to polymers [4–7]. The process of coarsening or phase ordering kinetics of a system starting from a random starting configuration to zero temperature, i.e., during a pure energy-minimization procedure, can be described and *classified* by a number of nonequilibrium exponents. One can directly observe the growth of ordered regions in every such process, which is quantified by estimating the characteristic length  $\ell(t)$  and the associated growth exponent  $\alpha$ . Another class of observations can be summarized under the term “persistence”, which is a concept directly related to the first-passage properties of systems [8]. It is defined only for quenches to  $T \equiv 0$ , although there have been attempts to also extract these properties from simulations at finite  $T$  [9, 10]. We investigate both those properties and related observables for the long-range Ising model with algebraically decaying interactions, for which very little is known both analytically and simulationally. This process is especially interesting at zero temperature, since exceptional behavior has been shown to often be observable under these special circumstances.

In the following Section II we first recall the models and present some scaling predictions, followed by a presentation of the used methods in Section III. Subsequently results are presented which are expected to be in the short-range regime of the long-range Ising model [11–17] in Section IV. Next, we will have a closer look at the long-range regime which are still treatable without too

overwhelming finite-size effects in Section V. The behavior for intermediate interaction strengths will be investigated in Section VI before concluding in Section VII.

## II. MODELS AND SCALING PREDICTIONS

The most studied model in coarsening phenomena is the nearest-neighbor Ising model (NNIM) with Hamiltonian

$$\mathcal{H} = -J \sum_{\langle ij \rangle} s_i s_j, \quad (1)$$

in  $d = 2$  spatial dimensions on a square lattice. In the Hamiltonian,  $s_i = \pm 1$  are the spins and  $J$  the coupling constant, where we fix  $J \equiv 1$  for ferromagnetic interactions. Here  $\langle ij \rangle$  symbolizes a summation over all nearest-neighbor pairs. The main system under consideration is an alteration, where every spin interacts with all other spins, the long-range Ising model (LRIM) with Hamiltonian

$$\mathcal{H} = -J \sum_{i < j} J(r_{ij}) s_i s_j, \quad (2)$$

Here  $J(r_{ij})$  is the power-law decaying potential of form

$$J(r_{ij}) = \frac{1}{r^{d+\sigma}}, \quad (3)$$

where  $s_i = \pm 1$  are again spins located on a square lattice in  $d = 2$  spatial dimension.

In most cases, the growth of the characteristic length is given by a power law

$$\ell(t) \sim t^\alpha, \quad (4)$$

where  $\alpha$  is the growth exponent. For the NNIM in  $d = 2$ , it is well established that the growth exponent is directly related to the dynamical exponent, i.e.,  $\alpha = 1/z$ , where

<sup>\*</sup> henrik.christiansen@itp.uni-leipzig.de

<sup>†</sup> suman.majumder@itp.uni-leipzig.de

<sup>‡</sup> wolfhard.janke@itp.uni-leipzig.de

the dynamical exponent  $z = 2$  for all quench temperatures  $T < T_c$ . On the other hand, in  $d = 3$  the zero temperature dynamics is severely finite-size effected, so that the asymptotic growth regime is hard to sample and one rather finds a smaller exponent, viz.,  $\alpha \approx 1/3$ . Only for system sizes of up to  $2048^3$ , i.e., more than 8 billion spins, one can clearly observe this growth law with  $\alpha = 1/2$  [18].

Persistence [19, 20] has been studied in various other contexts, ranging from random walk like systems [21–24] over surface growth [25–28] to disordered systems [28]. Its definition and methods have also found application to the description of economic data [29]. Some analytical and numerical predictions have been confirmed experimentally for liquid crystals [30], diffusive systems [31], and fluctuating steps [32]. Most studies have focused on the persistence probability

$$P(t) = 1 - \frac{N_f(t)}{V}, \quad (5)$$

where  $V = L^d$  is the volume of the system and  $N_f(t)$  quantifies the number of elements of the system that have had a first-passage in the time interval  $[0, t]$ , defining the first-passage time  $t$ . For the Ising model, a first-passage is defined as the first flip of a spin, i.e., the reversal of a local magnetic moment. For many systems, one finds a power-law decay of the persistence probability as a function of time,

$$P(t) \sim t^{-\theta}. \quad (6)$$

For the persistence exponent  $\theta$  there exist no exact estimates in  $d = 2$  dimensions, even for the NNIM [20]. For a quench from an uncorrelated starting configuration to  $T = 0$ , numerically a value of  $\theta = 0.22$  [33, 34] is found, whereas analytical approximations suggest  $\theta \approx 0.19$  [22, 35]. In the more recent analysis of Ref. [36] an influence of finite-time effects was recognized. Incorporating these effects led to an estimate of  $\theta = 0.198(3)$ , i.e., a value closer to the analytic approximation. Commonly, a value of  $\theta = 0.225$  is quoted [37, 38].

For some systems additional information may be extracted from investigating the correlation between persistent elements. In Ref. [39] it was for example noted that a flip of a spin at a given site at time  $t$  increases the chance of a neighboring spin flipping at time  $t' > t$ . This naturally implies a spatial correlation of persistent spins. They proposed to quantify these correlations by introducing the correlation function of persistent sites as

$$D(r, t) = \frac{\langle \rho(x, t) \rho(x + r, t) \rangle}{\langle \rho(x, t) \rangle}, \quad (7)$$

where  $\rho(x, t) = 1$  if site  $x$  is persistent and zero otherwise. The angular brackets  $\langle \dots \rangle$  denote the average over initial conditions and independent trajectories. With this definition, one has  $\langle \rho(x, t) \rangle = P(t)$ . A length scale of this persistent lattice,  $\ell_p(t)$ , quantifying the separation of correlated and uncorrelated regions, grows akin to the

length scale of the direct lattice  $\ell(t)$  as a power-law function of time as

$$\ell_p(t) \sim t^\alpha, \quad (8)$$

where  $\alpha$  is again the growth exponent.  $D(r, t)$  has the dynamic scaling relation

$$D(r, t) = P(t) f(r/\ell_p(t)). \quad (9)$$

One finds for the scaling function  $f(x)$

$$f(x) = D(r, t)/P(t) \sim \begin{cases} x^{-e} & x \ll 1 \\ 1 & x \gg 1 \end{cases}, \quad (10)$$

where  $x = r/\ell_p(t)$ . One can now use the property [40] that the two-point correlator is independent of  $t$  for  $r \ll \ell_p(t)$  (for a numerical confirmation see Fig. 2). The only relation guaranteeing this is requiring  $\ell_p^{-e} \sim t^{-\theta}$ . This implies  $D(r, t) \sim r^{-e}$  for  $\ell_p \gg r$  and plugging it into Eq. (8) one arrives at the scaling relation

$$e\alpha = \theta. \quad (11)$$

The exponent  $e$  is directly related to the fractal dimension as can be seen from analytically analyzing the number of persistent spins in the square grid, which yields the relation [39, 40]

$$d_f = d - e. \quad (12)$$

Combining Eqs. (11) and (12) one arrives at a relation between the nonequilibrium exponents given as

$$d_f - d = \theta/\alpha. \quad (13)$$

Inserting the extreme estimates of  $\theta$  into (11), one arrives at an *a priori* estimate of  $1.55 < d_f < 1.62$ . These bounds are in agreement with all values estimated in the literature for  $d_f$  [38, 40]. To conclude, for the NNIM one has:  $\alpha = 0.5$ ,  $0.19 < \theta < 0.225$ ,  $0.38 < e < 0.45$ , and  $1.55 < d_f < 1.62$ .

For the LRIM with Hamiltonian (2) system there exists a prediction of the asymptotic growth behavior reading  $\ell(t) \sim t^{1/(1+\sigma)}$  for  $\sigma < 1$  and  $\ell(t) \sim t^{1/2}$  for  $\sigma > 1$  with an additional multiplicative logarithmic correction at  $\sigma = 1$  [11–13]. This was derived using the deterministic time-dependent Ginzburg-Landau equation (without thermal contributions) and a continuous order parameter. Numerically, this prediction has been confirmed in the  $d = 2$  LRIM [14, 15] for quench temperature  $T = 0.1T_c \neq 0$  and subsequently in  $d = 1$  [16]. In  $d = 1$  it was found in Ref. [16] via a mapping to a two domain approximation and onto the one-dimensional convection-diffusion equation that, apart from above asymptotic growth law, one observes different initial growth regimes. The characteristic length of these regimes depends on  $\sigma$ ; at early times one observes a “ballistic” growth with  $\ell(t) \sim t$ , followed always by a regime where  $\ell(t) \sim t^{1/(1+\sigma)}$ , and finally only

for  $\sigma > 1$  one has  $\ell(t) \sim t^{1/2}$ . For long-range interacting systems in  $d = 1$  with any  $\sigma$  at  $T = 0$  only spins at domain boundaries can flip and will, within the framework of a two domain approximation, always lead to a growth of the bigger domain since this is energetically favorable. This means that at  $T = 0$  the ballistic regime becomes the asymptotic one and the other regimes are not observed. We expect in  $d = 2$  at  $T = 0$  a similar and  $\sigma$  independent growth law, although the value of the growth exponent can not be derived as in  $d = 1$ .

For the investigation of the persistence in long-range systems, only very little is known. There exists one study [41] which investigates the case of zero-temperature coarsening in the  $d = 1$  LRIM modeled via Langevin dynamics which observes the above mentioned asymptotic prediction and  $P(t) \sim \ell(t)^{-\bar{\theta}}$  with  $\bar{\theta} \approx 0.17507588$  as for the nearest-neighbor time-dependent Ginzburg-Landau equation [33, 42]. This corresponds trivially to  $P(t) \sim t^{-\alpha\bar{\theta}}$ , i.e., there a  $\sigma$  dependent persistence exponent  $\theta = \alpha\bar{\theta}$  was found. For the one-dimensional NNIM, one instead finds  $\theta = 3/8$  [43].

### III. METHODS

We simulate the LRIM with non-conserved order parameter in  $d = 2$  spatial dimensions with Hamiltonian (3) using Markov Chain Monte Carlo. When doing zero-temperature dynamics Monte Carlo, this algorithm degenerates to an energy minimization. A randomly chosen spin is flipped if the flip results in a lower energy of the system. If using the Glauber criterion, a spin-flip resulting in zero energy change is accepted with 50% probability. Using the Metropolis criterion, such a spin-flip is always accepted. For this work, we use the Glauber criterion, although in practice for systems with long-range interactions a proposed spin flip with zero energy change is very unlikely.

When simulating systems with long-range interactions, the needed computational resources for a given system size are significantly increased when compared to the short-range counterpart. We recently employed an approach where a simulation during a coarsening process is significantly sped up [14, 15]. Additionally, finite-size effects are very prominent in long-range interacting systems. Therefore we use Ewald summation to calculate the effective interactions  $J_{i,j}$  between spin  $i$  and  $j$  [44, 45], which are said to effectively reduce the effects of a finite system. Nonetheless, this still makes a careful treatment of finite-size effects in systems with strongly long-range interactions necessary, which we will put an emphasis on in Section V.

The length  $\ell(t)$  entering the asymptotic scaling law (4) is extracted by taking the intersection of the two-point equal-time correlation function

$$C(r, t) = \langle s_i(t)s_j(t) \rangle - \langle s_i(t) \rangle \langle s_j(t) \rangle \quad (14)$$

with a reasonable choice of a constant value in the range

$(0, 1)$  (here 0.5). The value of  $r$  at this intersection is then interpreted as the characteristic length  $\ell(t)$  at this time. When one now plots self-consistently  $C(r, t)$  versus  $r/\ell(t)$ , due to this being a scaling process, one expects the curve to collapse for all times  $t$  in the scaling regime. The calculation of this correlation function is numerically sped up via a fast Fourier transform.

All simulation results, apart from the snapshots, are obtained by averaging over at least 40 independent runs. This is realized by running the simulation with otherwise identical parameters for different random number generator seeds, corresponding to an average over different initial conditions and time evolutions. For reference, a single run of system size  $L = 4096$  takes roughly 3.5 weeks on 20 cores when parallelized with OpenMP.

For our fits, we make use of Jackknifing, i.e., when we have  $N$  independent runs, we also perform  $N$  fits each on data sets containing the information from  $N - 1$  runs. This allows us to calculate (reliable) error bars on the fit parameters by taking care of the (trivially) introduced correlation by using the same data many times [46].

### IV. SHORT-RANGE REGIME

Naively, one would expect to recover all exponents as in the NNIM for  $\sigma \rightarrow \infty$ . To check this, we first focus on the case of  $\sigma = 8$ , which for quenches to  $T \neq 0$  [14, 17] and in equilibrium [47, 48] undoubtedly corresponds to the short-range regime.

In Fig. 1 we first show snapshots of the direct (upper row) and persistence (lower row) lattice for  $t = 100, 200, 400$  from a single quench for system size  $L = 2048$  and  $\sigma = 8$ . As expected, we observe the growth of ordered structures. Here, we want to note a difference between the NNIM and this model. While for the NNIM roughly 1/3 of the simulations at zero temperature get stuck in (in principle meta stable) stripe-like configurations [49–52], this is much less likely in the LRIM. To be able to investigate any growth laws, we have to establish that the data for the correlation functions  $C(r, t)$  and  $D(r, t)$  fall on a master curve when properly rescaled. This exercise is shown in Fig. 2 for (a) the correlation function of the direct lattice  $C(r, t)$  and (b) the correlation function of the persistence lattice  $D(r, t)$  using Eq. (10) for times  $t = 100, 200, 400, 800, 1200$ . Both correlation functions collapse well; dynamic scaling is found and both  $\ell(t)$  and  $\ell_p(t)$  are properly estimated. The extraction of  $\ell_p$  is relatively straight forward, since  $D(r, t)$  has a clear minimum. We perform fits of the power law part of Eq. (10), where error bars are estimated using Jackknifing. The data considered is for  $t = 1200$  (the largest time also plotted in Fig. 2(b)) and in the range  $0.05 < r/\ell_p(t) < 0.5$ . We find  $e = 0.430(2)$  and  $\chi_r^2 = 2(1)$ , which is also shown as a solid line in Fig. 2(b). This corresponds via Eq. (12) to  $d_f = 1.570(2)$  in good agreement to the results observed in the NNIM [38, 40]. We want to stress that this estimate is not to be taken too seriously, because the data

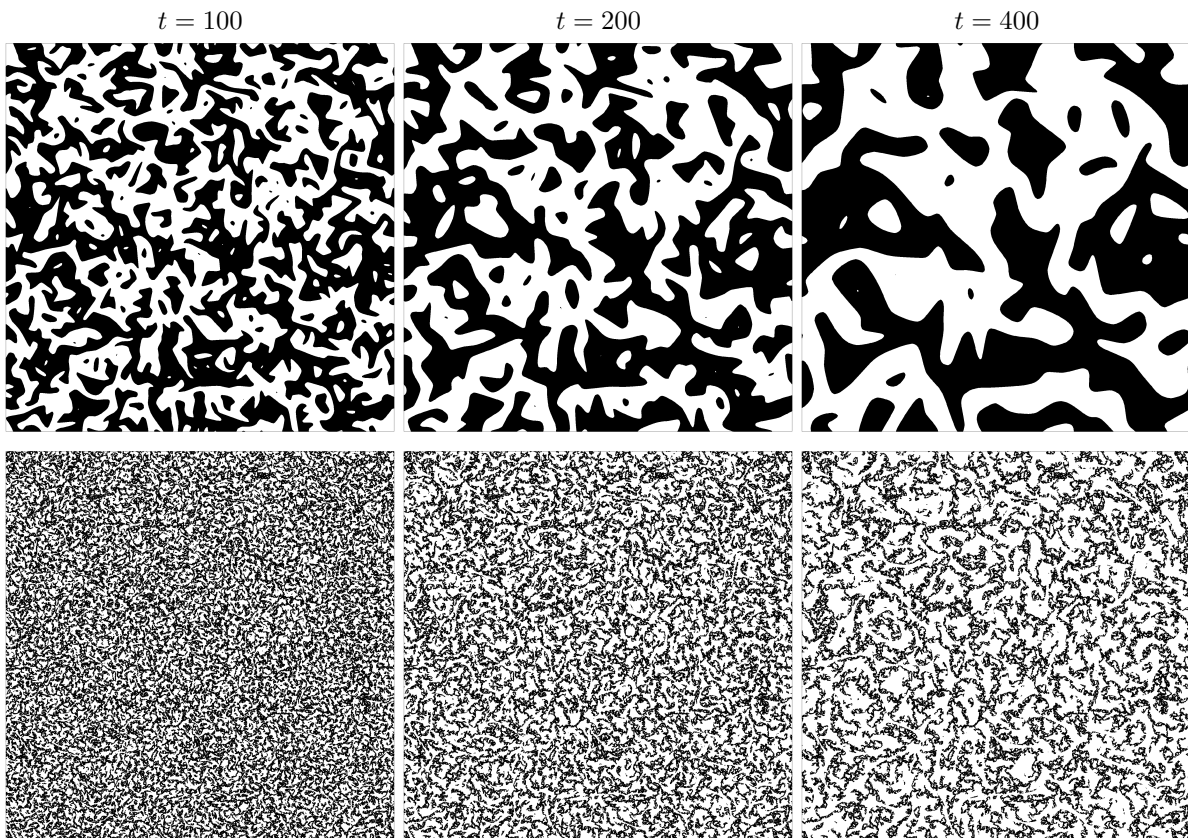


FIG. 1. Upper row: Configuration snapshots of the lattice after a quench from  $T = \infty$  to  $T = 0$  for a system size of  $L = 2048$  and for  $\sigma = 8$ . The growth of ordered regions is apparent as the time  $t = 100, 200, 400$  increases. Lower row: Corresponding snapshots from the same simulation of the persistent lattice for the identical times. The fractal structure of these configurations is clear.

is well compatible with a relatively wide range of  $e$  when only slightly adjusting the fitting range ( $0.42 < e < 0.44$  cannot be unambiguously ruled out), corresponding to  $1.56 < d_f < 1.58$ .

We next investigate both the length scales  $\ell(t)$  and  $\ell_p(t)$  already used as a rescaling factor in Fig. 3. We expect both of them to follow the same power law with growth exponent  $\alpha$ . In Fig. 3, both lengths are plotted against time  $t$  for  $\sigma = 8$  and  $L = 2048$ . To extract a numerical estimate of  $\alpha$ , we perform fits in the range  $10^2 < t < 10^3$ , giving  $\alpha = 0.743(9)$  with  $\chi_r^2 \approx 1$  for  $\ell$  and  $\alpha = 0.724(6)$  with  $\chi_r^2 \approx 0.4$  for  $\ell_p$ . These values are suggestively close to  $\alpha = 3/4$ , so that we plot as a dashed line a power-law with exponent  $\alpha = 3/4$ , which appears to be consistent with the data for both lengths. To further consolidate this, we plot  $\ell(t)/t^\alpha$ , which should be constant in the scaling region if this is the correct exponent. In the interval  $[10^2, 10^3]$ , this very much is the case, as could also be appreciated from a plot on normal scale (not shown). Finally, to confirm that both lengths follow the same power law, we plot  $\ell(t)/\ell_p(t)$  which correspondingly should be constant as well in this region. Within the available data accuracy this can be again easily ap-

preciated from the figure.

Finally, the persistence probability  $P(t)$  is presented in Fig. 4. To check the validity of Eq. (11) we calculate the value of  $\theta \approx 0.321$  from the fitted values, using  $\alpha$  extracted from  $\ell_p(t)$ . We also perform a fit in the range of  $10^2 < t < 10^3$  as before and find  $\theta = 0.321(2)$ . We cannot rule out a slightly different exponent  $0.31 < \theta < 0.34$ , however, the numeric value is very suggestive of the “nice” exponent  $1/3$  for  $\sigma \rightarrow \infty$ . Inserting  $\theta = 1/3$  and  $\alpha = 3/4$  into Eq. (11) gives a value of  $e = 0.4$  or  $d_f = 1.5$ . This value appears to be approximately compatible with the estimated value of  $d_f = 1.571$ . This approach is only a relatively weak numerical conjecture, but we nonetheless hope this to be suggestive for further analytical considerations.

It is surprising that we do not find  $\theta$  for  $\sigma = 8$  to be compatible with the value for the NNIM. The most robust exponent in this context appears to be the fractal dimension  $d_f$ , so that an universal fractal dimension for short-range models can be conjectured. As suggested by Eq. (11) a  $d_f$  compatible to the NNIM, but with a different growth exponent  $\alpha$ , implies a change of the persistence exponent  $\theta$ . To conclude, we conjecture that even for  $\sigma \rightarrow \infty$  (but still finite), the NNIM results are not

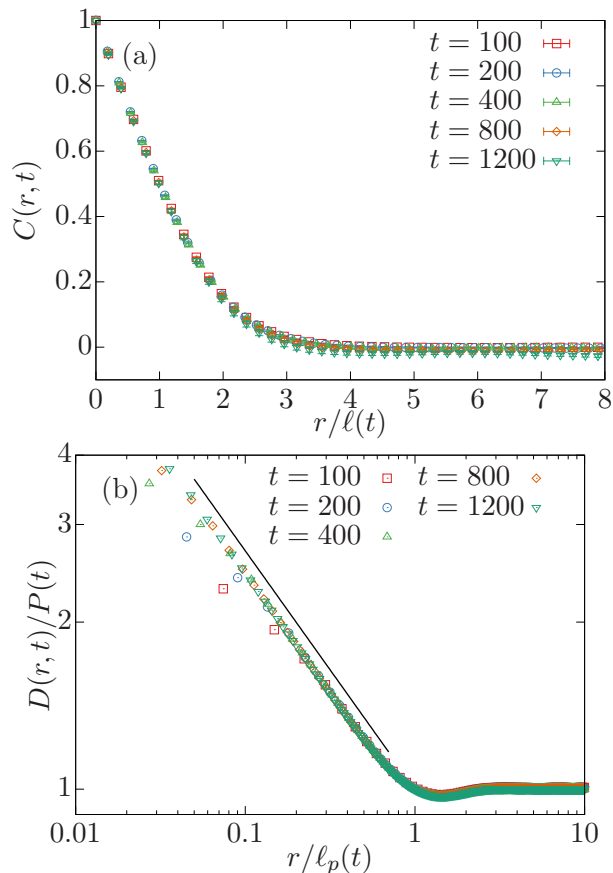


FIG. 2. (a) Correlation function of the direct lattice  $C(r,t)$  for  $\sigma = 8$  and  $L = 2048$  plotted against distance  $r$  scaled by the characteristic length  $\ell(t)$  extract from the intersection of this correlation function with 0.5 and (b) correlation function of the persistence lattice  $D(r,t)$  scaled by  $P(t)$  against the scaled distance  $r/\ell_p(t)$ , as described in Eq. (10) for times  $t = 100, 200, 400, 800, 1200$ . The solid line in (b) corresponds to a power law with exponent  $e = d - d_f = 0.43$ .

fully recovered for all exponents.

## V. LONG-RANGE REGIME

Because the results in the most short-range like case leads to *a priori* unexpected behavior, we now want to target stronger long-range interacting systems. We next focus on the most long-range case of  $\sigma = 0.6$  we can still treat without encountering too strong finite-size effects, using even larger lattices with  $L = 4096$  to avoid finite-size effects. Instead of combining the analysis for all other  $\sigma$  into a single section, we first focus on this case to be able to more carefully investigate this most difficult system, discussing the finite-size effects in more detail. Even smaller values of  $\sigma$  naturally lead to significantly more pronounced finite-size effects [17], so that even bigger system sizes than  $L = 4096$  would be needed. As the computing time increases as  $V^2$  ( $V = L^2$  is the total

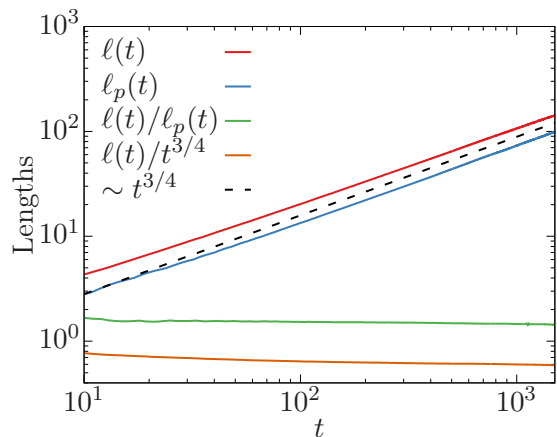


FIG. 3. The relevant lengths  $\ell(t)$  and  $\ell_p(t)$  for  $\sigma = 8$  and  $L = 2048$ . The statistical errors are of the order of the line width. The dashed black line corresponds to a power law in time  $t$  with growth exponent  $\alpha = 3/4$ . Additionally plotted is  $\ell(t)/\ell_p(t)$  which is expected to be constant as they both follow the same power law and  $\ell(t)/t^{3/4}$  which is also roughly constant in a relatively long time window, indicating that the growth also here follows  $\ell(t) \sim t^{3/4}$ .

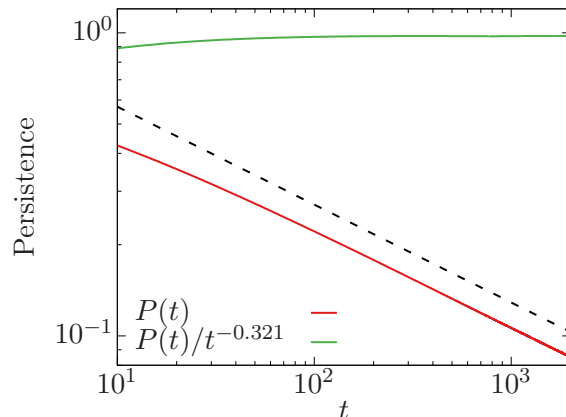


FIG. 4. Persistence probability  $P(t)$  versus time  $t$  for  $\sigma = 8$  and  $L = 2048$ . The dashed black line corresponds to a power law decay with exponent  $\theta = 0.321$ . To confirm that this exponent is compatible with the data, we have additionally plotted  $P(t)/t^{-\theta}$ .

number of spins) in terms of sweeps, the computing time would roughly increase by a factor of 16 per sweep and one would require roughly 4 times as many sweeps until finite-size effects are visible when doubling the system size. This is currently unfeasible, so that our smallest  $\sigma$  considered is 0.6.

We again start by investigating the snapshots of the direct and persistent lattice in Fig. 5. Again, the domains grow with time for the direct lattice, although the growth appears to be faster. Whether this is reflected in the growth exponent  $\alpha$  or the amplitude is *a priori* not clear. For the persistent lattice, it appears that the

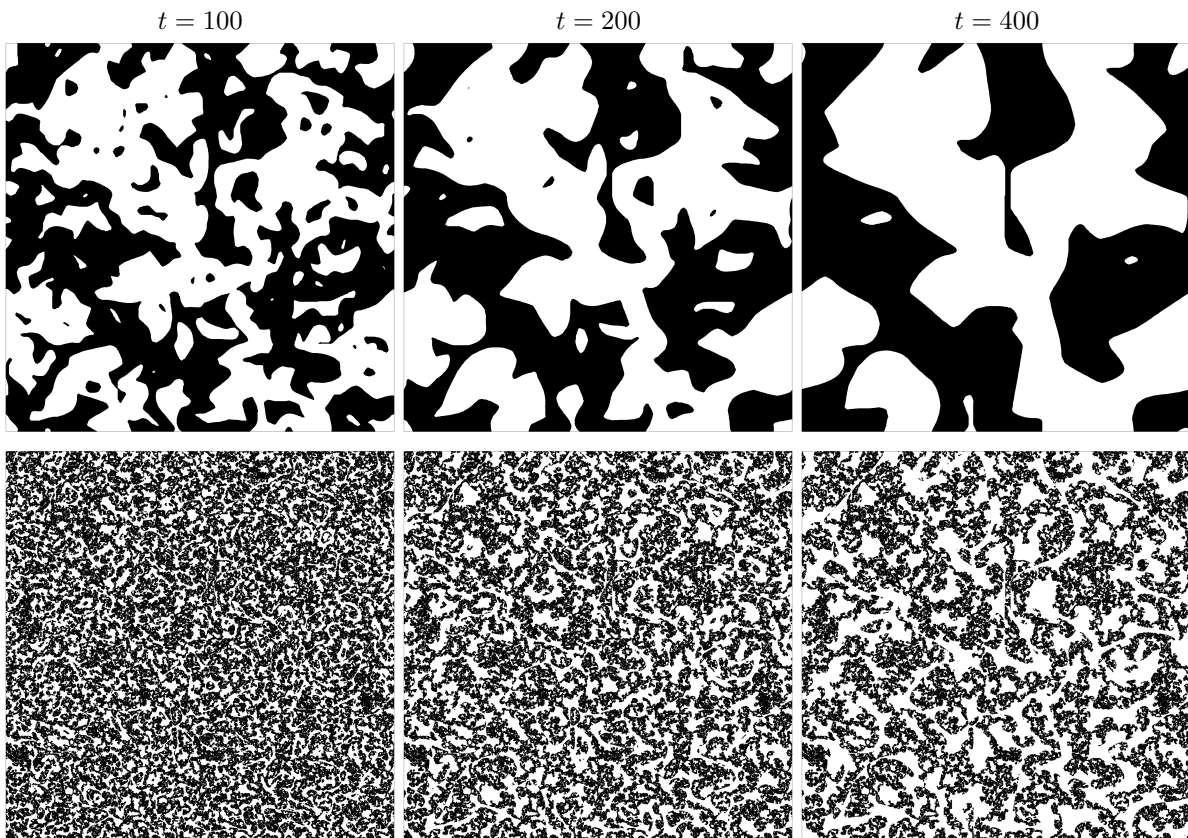


FIG. 5. Upper row: Configuration snapshots of the lattice after a quench from  $T = \infty$  to  $T = 0$  for a system size of  $L = 2048$  and for  $\sigma = 0.6$ . The growth of ordered regions is apparent as the time  $t = 100, 200, 400$  increases. Lower row: Corresponding snapshots from the same simulation of the persistent lattice for the identical times. The fractal structure of these configurations is clear.

persistent spins are more correlated. Also here, the dynamics appear to be faster.

We, however, first need to again establish that we are dealing with a scaling phenomenon. For this, we rescale both correlation functions in Figs. 6. While especially the scaling of the correlation function of the direct lattice  $C(r, t)$  in (a) is not as good as in Fig. 2(a), akin to what we observed already for quenches to  $T \neq 0$  ( $< T_c$ ) [14], we still observe satisfactory scaling for small  $r$ . For the persistent correlation function, this scaling appears better, although of course this is plotted on a log-log scale. An objective measure of collapse is very hard to obtain, thus we abstain ourselves from such an approach. Note that the form of  $D(r, t)$  of the persistent correlation function changed. While for  $\sigma = 8$  one sees a clear minimum around  $r/\ell_p \equiv 1$ , this minimum is much more shallow for  $\sigma = 0.6$ . This, apart from being an unexplained phenomenon, also has practical implications as extracting  $\ell_p(t)$  from the intersection with  $P(t)$  becomes slightly more difficult.

The solid line in Fig. 6(b) is a power law fitted to the data for  $t = 800$  in the range  $0.03 < r/\ell(t) < 0.5$ , giving  $e = d - d_f = 0.268(2)$  or  $d_f = 1.732(2)$ . This value of  $d_f$  is significantly different from  $d_f \approx 1.57$  found for the

NNIM or the LRIM with  $\sigma = 8$ . Already the snapshots of the persistent lattice in Fig. 5 indicated a different  $d_f$ , so that this does not come as a surprise.

We next focus on the direct length  $\ell(t)$  plotted for the three different system sizes in Fig. 7(a). The dashed black line is a power law with exponent  $\alpha = 3/4$ , which appears consistent with our data. A direct fit in the range from  $10^2 < t < 10^3$  provides  $\alpha = 0.720(7)$ . The finite-size effects become apparent from the earlier onset of a downward tendency of the data for smaller values of  $L$ . Note that the finite-size effects play a role even before they are visible in this figure. The dashed lines in the same color as the solid lines show  $\ell(t)/t^{3/4}$  to demonstrate that asymptotically the data is consistent with this exponent, as the region with a constant value increases for increasing system size.

The finite-size effects in Fig. 7(b) manifest by a deviation from the master curve towards higher values of  $\ell_p(t)$ . These effects are similar to the finite-size effects for the direct length  $\ell(t)$ , but in opposite direction, i.e., towards higher values and not lower values. Performing a fit in the range  $100 < t < 750$  for  $\ell_p$  gives  $\alpha = 0.773(5)$ . Here, also, we instead plot as a dashed black line a power law with exponent  $\alpha = 3/4$  and the dashed lines in the same

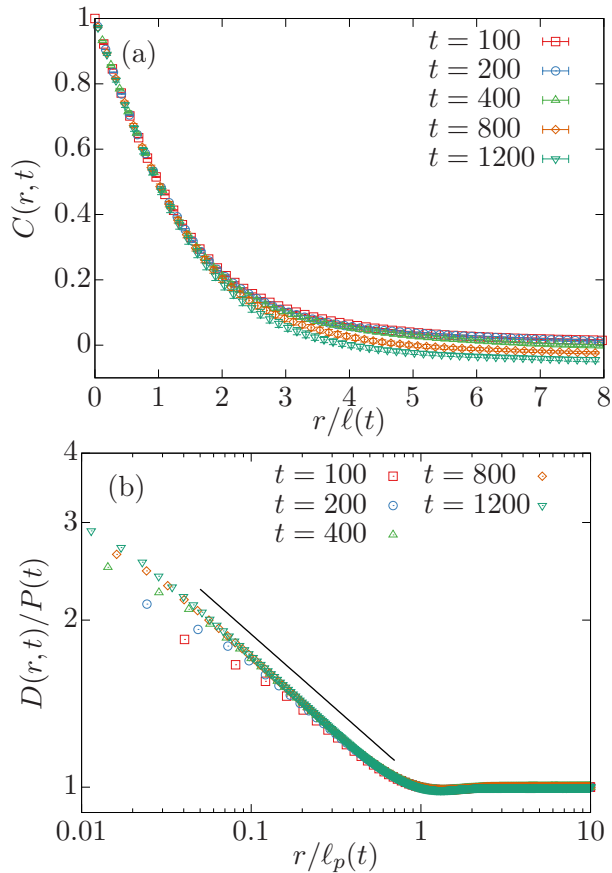


FIG. 6. (a) Correlation function of the direct lattice  $C(r, t)$  for  $\sigma = 0.6$  and  $L = 4096$  plotted against distance  $r$  scaled by the characteristic length  $\ell(t)$  extract from the intersection of this correlation function with 0.5 and (b) correlation function of the persistence lattice  $D(r, t)$  scaled by  $P(t)$  against the scaled distance  $r/\ell_p(t)$  for times  $t = 100, 200, 400, 800, 1200$ . The solid line in (b) corresponds to a power law with exponent  $e = d - d_f = 0.268$ .

color as the original data are  $\ell_p(t)/t^{3/4}$ . There exists a region where  $\ell_p(t)/t^{3/4}$  is constant. Thus we conclude that also in this case, the growth exponent is approximately given by  $\alpha \approx 3/4$ .

In Fig. 8 we show the persistence probability for the different  $L$  and  $\sigma = 0.6$ . The solid black line is a power law  $\sim t^{-\theta}$ , where  $\theta = 0.201(8)$  was obtained by plugging in  $e = 0.268(1)$  and  $\alpha = 0.75(3)$  (assuming an “arbitrary” but realistic error on  $\alpha$ ) into Eq. (11). Our persistence data is compatible with this law from roughly  $t \approx 30$  to  $t \approx 500$ . To consolidate this, as before we plot  $P(t)/t^{-\theta}$  as dashed lines, which confirms our previous observation. The data is approximately constant in this time frame. Of course using for example  $\alpha$  estimated from the growth of  $\ell_p$  or  $\alpha = 3/4$  changes this estimate of  $\theta$  significantly (up to  $\theta = 0.214(2)$ ). Performing a fit in the range  $10^2 < t < 10^3$  gives  $\theta = 0.219(1)$ .

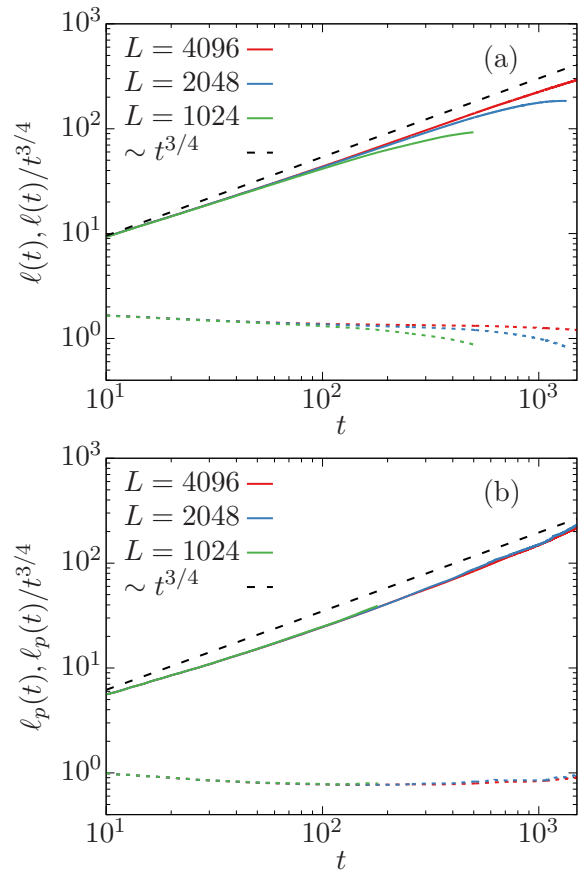


FIG. 7. (a) Characteristic length  $\ell(t)$  for  $\sigma = 0.6$  and  $L = 1024, 2048$ , and  $L = 4096$  as solid colored lines. The statistical errors are of the order of the line width. The dashed black line corresponds to a power law in time  $t$  with growth exponent  $\alpha = 3/4$ . Additionally plotted is  $\ell(t)/t^{3/4}$  for all system sizes in colored dashed lines, which for the correct scaling law should approach a constant. (b) Similar as (a), but for  $\ell_p(t)$ .

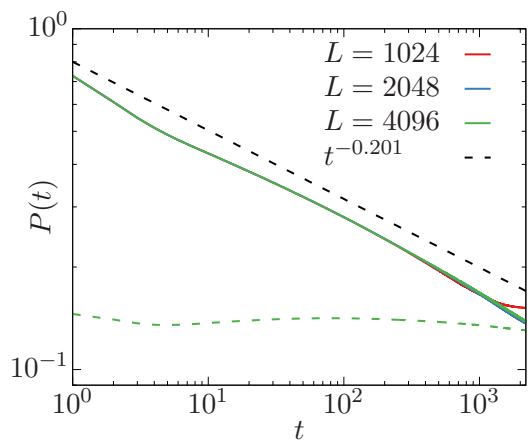


FIG. 8. Persistence probability  $P(t)$  versus time  $t$  for  $\sigma = 0.6$  and  $L = 1024, 2048, 4096$ . The dashed black line corresponds to a power law decay with exponent  $\theta = 0.201$ . To confirm that this exponent is compatible with the data, we have additionally plotted  $P(t)/t^{-\theta}$  as green dashed line for  $L = 4096$ .

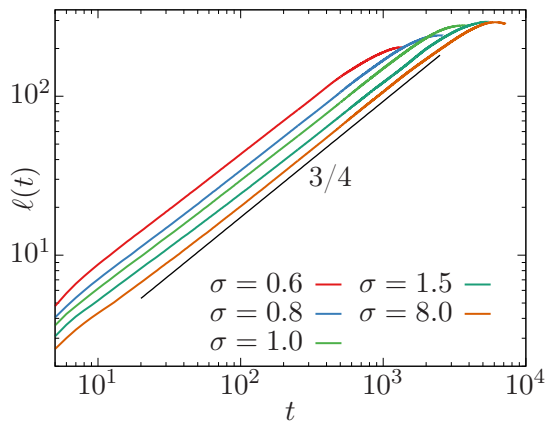


FIG. 9. Direct length  $\ell(t)$  for different values of  $\sigma \in [0.6, 8]$  with system size  $L = 2048$ . The solid black line corresponds to a power law  $\propto t^\alpha$ , with growth exponent  $\alpha = 3/4$  as estimated before.

## VI. DIFFERENT $\sigma$

We now focus on the behavior for  $\sigma$  in between the two extremes studied before, covering a wide range of interactions. In Fig. 9 we plot the direct length  $\ell(t)$  on a log-log plot for  $\sigma = 0.6, 0.8, 1.0, 1.5$ , and  $8$ . It is apparent that all data are more or less parallel to each other in a relatively long region and thus the estimate of  $\alpha = 3/4$  for all  $\sigma$  is compatible with the data.

In Table I we present data from power-law fits of form (10), giving estimates for  $d_f$  and the goodness of fit given by the reduced chi-square  $\chi_r^2 = \chi^2/\text{DOF}$ , where DOF denotes the degrees of freedom. We perform the fits in the range  $r_{\min}/\ell(t)$  to  $r_{\max}/\ell(t)$ , where we vary  $r_{\min}/\ell(t)$  and set  $r_{\max}/\ell(t) = 0.5$  for all  $\sigma$ . We also give the time  $t$  used, which we want to choose as big as possible without experiencing finite-size effects, so that we chose  $t = 800$  for  $\sigma \leq 1.5$  and  $t = 1200$  otherwise. In part,  $\chi_r^2$  is relatively big for  $\sigma = 0.6$  and  $\sigma = 0.8$ , but since we have carefully estimated the finite-size effects in the previous section, we are confident that these fits are nonetheless appropriate.

To get a better idea of the functional dependency obtained for the exponents, we plot  $d_f$  versus  $\sigma$  in Fig. 10(a). From our results for quenches to  $T \neq 0$ , one would expect some kind of transition at  $\sigma = 1$ , whereas from equilibrium studies one could expect a transition at  $\sigma = 2$  [47] or  $\sigma = 1.75$  [48]. The correct value for the crossover from the intermediate to short-range regime in equilibrium is still disputed in the literature [45, 53–57]. In our setting, however, no distinct crossover at any  $\sigma$  is observed. Thus one has to conclude, that this equilibrium phase transition does not manifest itself in the nonequilibrium dynamical behavior at  $T = 0$ . We rather observe a smooth approach of  $d_f$  to a value compatible with the NNIM fractal dimension. There exists no analytical background what kind of functional dependency one can expect here, thus we abstain ourselves from such

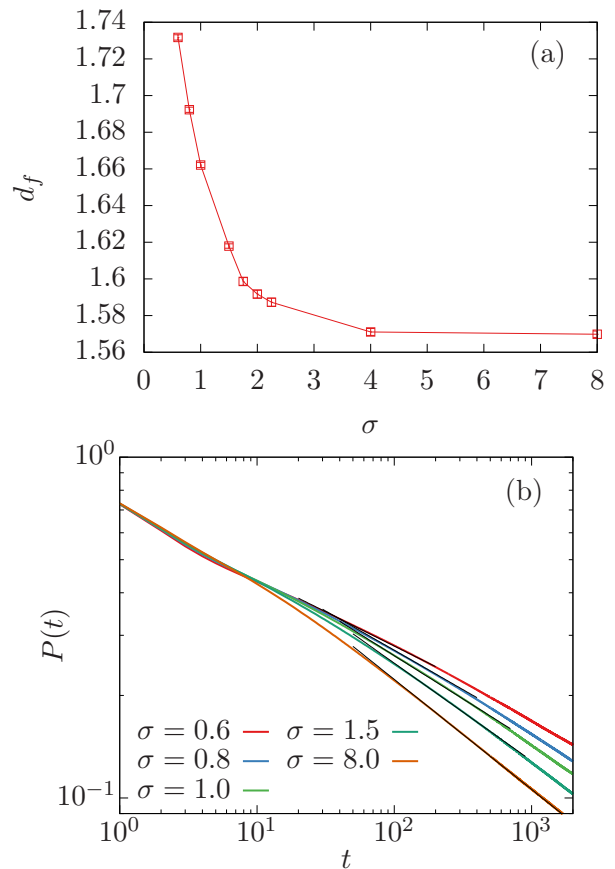


FIG. 10. (a) Fractal dimension  $d_f$  against  $\sigma$  as compiled in Table I. (b) Persistence probability  $P(t)$  for different  $\sigma$  versus time  $t$ . The solid black lines are power laws with exponent  $\theta$ , where  $\theta$  was obtained from Eqs. (11) and (13) by plugging in the values of  $d_f$  from Table I and using  $\alpha = 3/4$ .

an attempt to find an analytical form.

In Fig. 10(b) we show the persistence probability  $P(t)$  for different  $\sigma$ . We use Eq. (13) to obtain estimates for  $\theta$ , for which power laws with the obtained  $\theta$  are plotted as solid black lines. For a relatively large range, the power laws are consistent with the data for  $P(t)$ . Of course, the scaling regime gets smaller the smaller  $\theta$  is. Having considered the finite-size effects carefully, we are confident that the values for the exponents we quote are the true asymptotic values for all  $\sigma$ .

## VII. CONCLUSION

We have studied the zero-temperature coarsening of the long-range Ising model by tuning the degree of the long-range interactions via the power-law exponent  $\sigma$ . It is found that the growth exponent  $\alpha \approx 3/4$  is independent of  $\sigma$ . For our most short-range like case of  $\sigma = 8$ , we find that the fractal dimension is compatible to the value found for the nearest-neighbor Ising model and reads  $d_f \approx 1.57$ . Evidence was provided in favor of the

TABLE I. Values of the fractal dimension  $d_f$  from power-law fits of form  $f(x) = ax^{d_f-d}$  to the data for different  $\sigma$ . We fix the upper bound of the fitting range to  $r_{\max}/\ell(t) = 0.5$  and vary the lower bound  $r_{\min}/\ell(t)$ , where the corresponding values are noted in the table. The time used for the fit was varied from  $t = 800$  to  $t = 1200$  to allow for the longest, but still finite-size unaffected, regime. Mentioned are also the reduced chi-square  $\chi_r^2$ , indicating the goodness of fit. To be able to quantitatively compare the resulting values for  $\theta$  using Eq. (13) (assuming  $\alpha = 0.75(3)$  with “guessed” error bars) with the values obtained from a fit  $\theta_f$ , we have included both in the table. For  $\theta_f$ , we have also included the corresponding fitting ranges.

$\sigma$	0.60	0.80	1.00	1.50	1.75	2.00	2.25	4.00	8.00
$d_f$	1.732(2)	1.692(2)	1.662(2)	1.618(2)	1.599(3)	1.592(3)	1.587(3)	1.571(2)	1.570(2)
$t$	800	800	800	800	1200	1200	1200	1200	1200
$r_{\min}/\ell(t)$	0.03	0.05	0.1	0.15	0.15	0.15	0.15	0.15	0.15
$\chi_r^2$	6(2)	5(2)	1.4(5)	1.1(3)	3(2)	3(1)	3(2)	1.1(7)	1.9(9)
$\theta = (d_f - d)\alpha$	0.201(8)	0.231(9)	0.25(1)	0.29(1)	0.30(1)	0.31(1)	0.31(1)	0.32(1)	0.32(1)
$\theta_f$	0.1998(5)	0.2315(9)	0.258(1)	0.288(1)	0.288(1)	0.302(1)	0.299(1)	0.317(1)	0.319(1)
Fitting range of $\theta_f$	[20, 200]	[30, 400]	[40, 700]	[50, 900]	[50, 900]	[50, 950]	[50, 950]	[50, 950]	[50, 1000]

relation  $d - d_f = \theta/\alpha$ , which relates the nonequilibrium exponents. Here  $\theta$  is the persistence exponent and  $d$  is the spatial dimension. For  $\sigma = 8$ , we find  $\theta \approx 0.321$ , which is significantly different from the value for the nearest-neighbor Ising model with  $\theta \approx 0.2$ .

In the most long-range like system under consideration with  $\sigma = 0.6$ , we find that above relation relating the nonequilibrium exponents still is valid. Here, we find  $d_f \approx 1.732$  and thus  $\theta \approx 0.201$ . The value of  $\theta$  is most probably only coincidentally close to the nearest-neighbor Ising model value.

Finally, when investigating a whole number of  $\sigma$  in above range, one finds that  $d_f$  (and thereby  $\theta$ ) varies continuously with  $\sigma$ . There does not appear to be any distinct crossover.

As a further direction of investigation, one could redo this kind of analysis also in  $d = 1$  and  $d = 3$  dimensions. Such an endeavor could be even helpful in (more accurate) estimates of the fractal dimension exponents found

in the short-range Ising model in  $d = 3$  at zero temperature, where finite-size effects are enormous, since much less simulation get trapped in (meta-) stable configurations and the ground state is reached much more often.

After completion of this work, we became aware of the very recent preprint [58] where the authors also find  $\ell(t) \sim t^{3/4}$  independent of  $\sigma$ .

## ACKNOWLEDGMENTS

This project was funded by the Deutsche Forschungsgemeinschaft (DFG, German Research Foundation) under project No. 189853844 – SFB/TRR 102 (project B04), and the Deutsch-Französische Hochschule (DFH-UFA) through the Doctoral College “ $\mathbb{L}^4$ ” under Grant No. CDFA-02-07. We further acknowledge support by the Leipzig Graduate School of Natural Sciences “Build-MoNa”.

- 
- [1] A. J. Bray, Theory of phase-ordering kinetics, *Adv. Phys.* **51**, 481 (2002).
  - [2] S. Puri and V. Wadhawan, eds., *Kinetics of Phase Transitions* (CRC Press, Boca Raton, 2009).
  - [3] P. L. Krapivsky, S. Redner, and E. Ben-Naim, *A Kinetic View of Statistical Physics* (Cambridge University Press, Cambridge, United Kingdom, 2010).
  - [4] S. Majumder and W. Janke, Cluster coarsening during polymer collapse: Finite-size scaling analysis, *Europhys. Lett.* **110**, 58001 (2015).
  - [5] H. Christiansen, S. Majumder, and W. Janke, Coarsening and aging of lattice polymers: Influence of bond fluctuations, *J. Chem. Phys.* **147**, 094902 (2017).
  - [6] S. Majumder, J. Zierenberg, and W. Janke, Kinetics of polymer collapse: Effect of temperature on cluster growth and aging, *Soft Matter* **13**, 1276 (2017).
  - [7] S. Majumder, H. Christiansen, and W. Janke, Understanding nonequilibrium scaling laws governing collapse of a polymer, *Eur. Phys. J. B* **93**, 1 (2020).
  - [8] S. Redner, *A Guide to First-Passage Processes* (Cambridge University Press, Cambridge, United Kingdom, 2001).
  - [9] B. Derrida, How to extract information from simulations of coarsening at finite temperature, *Phys. Rev. E* **55**, 3705 (1997).
  - [10] S. Cueille and C. Sire, Spin block persistence at finite temperature, *J. Phys. A* **30**, L791 (1997).
  - [11] A. J. Bray, Domain-growth scaling in systems with long-range interactions, *Phys. Rev. E* **47**, 3191 (1993).
  - [12] A. J. Bray and A. D. Rutenberg, Growth laws for phase ordering, *Phys. Rev. E* **49**, R27 (1994).
  - [13] A. D. Rutenberg and A. J. Bray, Phase-ordering kinetics of one-dimensional nonconserved scalar systems, *Phys. Rev. E* **50**, 1900 (1994).
  - [14] H. Christiansen, S. Majumder, and W. Janke, Phase ordering kinetics of the long-range Ising model, *Phys. Rev. E* **99**, 011301(R) (2019).
  - [15] W. Janke, H. Christiansen, and S. Majumder, Coarsening in the long-range Ising model: Metropolis versus Glauber

- criterion, *J. Phys. Conf. Ser.* **1163**, 012002 (2019).
- [16] F. Corberi, E. Lippiello, and P. Politi, One dimensional phase-ordering in the Ising model with space decaying interactions, *J. Stat. Phys.* **176**, 512 (2019).
- [17] H. Christiansen, S. Majumdar, M. Henkel, and W. Janke, Aging in the long-range Ising model, *Phys. Rev. Lett.* **125**, 180601 (2020).
- [18] D. Gessert, H. Christiansen, and W. Janke, in preparation.
- [19] S. N. Majumdar, Persistence in nonequilibrium systems, *Curr. Sci.* **77**, 370 (1999).
- [20] A. J. Bray, S. N. Majumdar, and G. Schehr, Persistence and first-passage properties in nonequilibrium systems, *Adv. Phys.* **62**, 225 (2013).
- [21] S. N. Majumdar, C. Sire, A. J. Bray, and S. J. Cornell, Nontrivial exponent for simple diffusion, *Phys. Rev. Lett.* **77**, 2867 (1996).
- [22] S. N. Majumdar and C. Sire, Survival probability of a Gaussian non-Markovian process: Application to the  $T = 0$  dynamics of the Ising model, *Phys. Rev. Lett.* **77**, 1420 (1996).
- [23] M. Bauer, C. Godreche, and J. Luck, Statistics of persistent events in the binomial random walk: Will the drunken sailor hit the sober man?, *J. Stat. Phys.* **96**, 963 (1999).
- [24] G. Ehrhardt, S. N. Majumdar, and A. J. Bray, Persistence exponents and the statistics of crossings and occupation times for Gaussian stationary processes, *Phys. Rev. E* **69**, 016106 (2004).
- [25] J. Krug, H. Kallabis, S. Majumdar, S. Cornell, A. J. Bray, and C. Sire, Persistence exponents for fluctuating interfaces, *Phys. Rev. E* **56**, 2702 (1997).
- [26] H. Kallabis and J. Krug, Persistence of Kardar-Parisi-Zhang interfaces, *Europhys. Lett.* **45**, 20 (1999).
- [27] M. Constantin, S. Das Sarma, C. Dasgupta, O. Bondarchuk, D. Dougherty, and E. Williams, Infinite family of persistence exponents for interface fluctuations, *Phys. Rev. Lett.* **91**, 086103 (2003).
- [28] M. Constantin, C. Dasgupta, P. P. Chatrathorn, S. N. Majumdar, and S. Das Sarma, Persistence in nonequilibrium surface growth, *Phys. Rev. E* **69**, 061608 (2004).
- [29] F. Ren and B. Zheng, Generalized persistence probability in a dynamic economic index, *Phys. Lett. A* **313**, 312 (2003).
- [30] B. Yurke, A. Pargellis, S. Majumdar, and C. Sire, Experimental measurement of the persistence exponent of the planar Ising model, *Phys. Rev. E* **56**, R40 (1997).
- [31] G. P. Wong, R. W. Mair, R. L. Walsworth, and D. G. Cory, Measurement of persistence in 1D diffusion, *Phys. Rev. Lett.* **86**, 4156 (2001).
- [32] D. Dougherty, I. Lyubintsky, E. Williams, M. Constantin, C. Dasgupta, and S. Das Sarma, Experimental persistence probability for fluctuating steps, *Phys. Rev. Lett.* **89**, 136102 (2002).
- [33] B. Derrida, A. J. Bray, and C. Godreche, Non-trivial exponents in the zero temperature dynamics of the 1D Ising and Potts models, *J. Phys. A* **27**, L357 (1994).
- [34] D. Stauffer, Ising spinodal decomposition at  $T = 0$  in one to five dimensions, *J. Phys. A* **27**, 5029 (1994).
- [35] C. Sire, S. N. Majumdar, and A. Rüdinger, Analytical results for random walk persistence, *Phys. Rev. E* **61**, 1258 (2000).
- [36] T. Blanchard, L. F. Cugliandolo, and M. Picco, Persistence in the two dimensional ferromagnetic Ising model, *J. Stat. Mech.* **2014**, P12021 (2014).
- [37] J. Ye, J. Machta, C. Newman, and D. Stein, Nature versus nurture: Predictability in low-temperature Ising dynamics, *Phys. Rev. E* **88**, 040101 (2013).
- [38] S. Chakraborty and S. Das, Fractality in persistence decay and domain growth during ferromagnetic ordering: Dependence upon initial correlation, *Phys. Rev. E* **93**, 032139 (2016).
- [39] G. Manoj and P. Ray, Scaling and fractal formation in persistence, *J. Phys. A* **33**, L109 (2000).
- [40] S. Jain and H. Flynn, Scaling and persistence in the two-dimensional Ising model, *J. Phys. A* **33**, 8383 (2000).
- [41] I. Ispolatov, Persistence in systems with algebraic interaction, *Phys. Rev. E* **60**, R2437 (1999).
- [42] A. Bray, B. Derrida, and C. Godreche, Non-trivial algebraic decay in a soluble model of coarsening, *Europhys. Lett.* **27**, 175 (1994).
- [43] B. Derrida, V. Hakim, and V. Pasquier, Exact first-passage exponents of 1D domain growth: Relation to a reaction-diffusion model, *Phys. Rev. Lett.* **75**, 751 (1995).
- [44] P. Ewald, Die Berechnung optischer und elektrostatischer Gitterpotentiale, *Ann. Phys. (Berl.)* **369**, 253 (1921).
- [45] T. Horita, H. Suwa, and S. Todo, Upper and lower critical decay exponents of Ising ferromagnets with long-range interaction, *Phys. Rev. E* **95**, 012143 (2017).
- [46] B. Efron, *The Jackknife, the Bootstrap and Other Resampling Plans* (Society for Industrial and Applied Mathematics, Philadelphia, 1982).
- [47] M. E. Fisher, S.-k. Ma, and B. Nickel, Critical exponents for long-range interactions, *Phys. Rev. Lett.* **29**, 917 (1972).
- [48] J. Sak, Recursion relations and fixed points for ferromagnets with long-range interactions, *Phys. Rev. B* **8**, 281 (1973).
- [49] S. Safran, P. S. Sahni, and G. S. Grest, Kinetics of ordering in two dimensions. I. Model systems, *Phys. Rev. B* **28**, 2693 (1983).
- [50] V. Spirin, P. Krapivsky, and S. Redner, Fate of zero-temperature Ising ferromagnets, *Phys. Rev. E* **63**, 036118 (2001).
- [51] V. Spirin, P. Krapivsky, and S. Redner, Freezing in Ising ferromagnets, *Phys. Rev. E* **65**, 016119 (2001).
- [52] T. Blanchard and M. Picco, Frozen into stripes: Fate of the critical Ising model after a quench, *Phys. Rev. E* **88**, 032131 (2013).
- [53] E. Luijten and H. W. Blöte, Boundary between long-range and short-range critical behavior in systems with algebraic interactions, *Phys. Rev. Lett.* **89**, 025703 (2002).
- [54] M. Picco, Critical behavior of the Ising model with long range interactions, arXiv preprint arXiv:1207.1018 (2012).
- [55] T. Blanchard, M. Picco, and M. Rajabpour, Influence of long-range interactions on the critical behavior of the Ising model, *Europhys. Lett.* **101**, 56003 (2013).
- [56] M. C. Angelini, G. Parisi, and F. Ricci-Tersenghi, Relations between short-range and long-range Ising models, *Phys. Rev. E* **89**, 062120 (2014).
- [57] N. Defenu, A. Trombettoni, and A. Codello, Fixed-point structure and effective fractional dimensionality for  $O(N)$  models with long-range interactions, *Phys. Rev. E* **92**, 052113 (2015).
- [58] R. Agrawal, F. Corberi, E. Lippiello, P. Politi, and S. Puri, Kinetics of the two-dimensional long-

range Ising model at low temperatures, arXiv preprint  
arXiv:2011.05030 (2020).